PAPER • **OPEN ACCESS**

Plasma parameters analysis in DC and RF magnetron sputtering using finite element method

To cite this article: Noely Z Calderón *et al* 2025 *Phys. Scr.* **100** 105604

Physica Scripta

OPEN ACCESS

RECEIVED
29 May 2025

REVISED
9 September 2025

ACCEPTED FOR PUBLICATION
26 September 2025

PUBLISHED
9 October 2025

PAPER

Plasma parameters analysis in DC and RF magnetron sputtering using finite element method

Noely Z Calderón[1,2,*], Carlo Becerra[3], Jose Campo[3], Jean Carrreño[3], Humberto Torreblanca[4,5], Michael Stüber[2], Sven Ulrich[2] and Rolf Grieseler[1]

[1] Science Department, Physisc section, Pontificia Universidad Católica del Perú, Av. Universitaria 1801, Lima 32, Peru
[2] Institute for Applied Materials-Applied Materials Physics (IAM-AWP), Karlsruhe Institute of Technology, 76131 Karlsruhe, Germany
[3] Universidad Nacional de Ingeniería, Av. Túpac Amaru 210, Lima, Peru
[4] Ecole Polytechnique Fédérale de Lausanne (EPFL), Swiss Plasma Center (SPC), Lausanne CH-1015, Switzerland
[5] Current affiliation: Type One Energy Group, 40 New York Avenue, Oak Ridge, TN, USA.
[*] Author to whom any correspondence should be addressed.

E-mail: noely.calderon@pucp.edu.pe

Keywords: magnetron sputtering, FEM, glow discharge, plasma modelling, thin film

Abstract

A comprehensive comparison of results obtained by finite element modelling (FEM) and plasma diagnostics between direct current (d.c.) and radio frequency (RF) magnetron sputtering at a frequency of 13.56 MHz is presented. This research studies the influence of power in the range 20 W to 90 W at a constant argon gas pressure of 1 Pa. The maximum plasma density values are observed at 90 W in the d.c. mode, reaching 1.41×10^{17} m^{-3}, and 1.95×10^{16} m^{-3} in the RF mode, with results obtained within 1 μs after ignition of the plasma. The results of the experiments showed that the plasma concentration at a distance of 23 mm from the cathode has maximum values; indicating that the electron and ion density values increase as the d.c. and RF magnetron sputtering power increases. This research aims to demonstrate the different charge density values obtained in RF and d.c. plasma with FEM to facilitate the prediction of the magnetron sputtering discharge parameters of the MatER PUCP laboratory. Given that at this moment suitable models for RF sputtering are rather scarce, the obtained plasma parameters from FEM will be compared to plasma parameters that were obtained experimentally.

1. Introduction

As technology advances, industrial applications of plasma have grown exponentially, becoming a key resource in various sectors. From surface treatment to improve material adhesion and durability to its use in thin film deposition in the semiconductor industry, plasma plays an important role in process and product optimization. Plasma is particularly noticeable in magnetron sputtering, a technique involving magnetic and electric fields to produce discharges with fundamental applications in thin film development [1–4]. Moreover, different types of magnetron sputtering equipment worldwide are being used to form thin films due to their ability to deposit uniform and specific layers of material on diverse surfaces. This technique relies most importantly on parameters such as pressure in the vacuum chamber, applied power, the magnetic field at the magnetrons, applied bias to the substrate, as well as the temperature and other parameters which can modify the structure of the deposited thin film [5, 6].

This process can lead to high-purity coatings in a range between a few nanometers and up to several microns. For this, a target material is sputtered due to the impact of highly energetic ions. Subsequently, the sputtered material forms the desired coating on a substrate. The ionization probability for these ejected target ions is relatively low (less than 10%); thus, the deposited species remain neutral [7]. Sputtering occurs within a chamber filled with a working gas, typically argon (Ar). In figure 1, a schematic of the magnetron sputtering system is shown. The system employs an RF magnetron cathode within a vacuum chamber of approximately $50 \times 53 \times 54$ cm^3 in volume. The base pressure during operation is maintained around 1×10^{-4} Pa. These

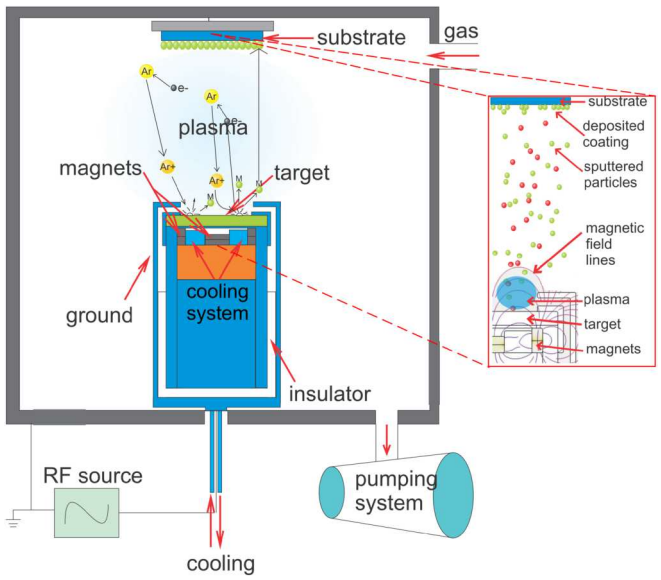

Figure 1. Setup of the RF magnetron sputtering chamber and the ionization process of the working gas (e.g. argon).

Table 1. Experimental data used in the MaTER PUCP laboratory.

Parameter	Value
Base Pressure	1×10^{-4} Pa
Working Pressure	1 Pa
Target–substrate distance	7 cm
Working gas	Argon 99.999%(*purity*)
RF power source	0–90 W
Chamber volume	$50 \times 53 \times 54 cm^3$

parameters define the experimental conditions upon which the simulations are based (table 1). Furthermore, the collision of the ions with the target causes the ejection of elemental atoms which are subsequently deposited on the substrate. The target is connected to the RF or d.c. source, and for this study, it is assumed to be aluminum [3].

In recent years, the accurate modeling of low-pressure plasmas has become increasingly important for both fundamental studies and technological applications. While particle-in-cell (PIC) methods offer a detailed and physically accurate representation of plasma behavior, they are computationally expensive and often impractical for large-scale or long-duration simulations. As an alternative, fluid models have been widely used due to their lower computational cost. About a decade ago, COMSOL Multiphysics enabled fluid-based plasma simulations for pressures above 10 Pa. Recent improvements in the numerical implementation allow these models to be applied to pressures as low as 1 Pa. However, at such low pressures, fluid models begin to reach their physical and numerical limitations, thus requiring careful validation of the results. To ensure the reliability of simulation outcomes, comparison with experimental plasma diagnostics is essential. In most cases, agreement at a single point—typically near the substrate—is sufficient to validate the model, allowing extrapolation of the results to the entire plasma volume. Nevertheless, comprehensive plasma diagnostics across the entire discharge space are not only time-consuming but often infeasible in certain regions, such as near the target, where probe-induced perturbations or electrical discharges may occur [8–12]. For example, Ayub *et al* performed in-situ plasma characterization of DC/RF magnetron sputtering using Langmuir probe and optical emission spectroscopy, analyzing key plasma parameters such as electron density, electron temperature, and plasma potential. Their results highlight the importance of experimental diagnostics for optimizing sputtering processes and improving film quality [13].

Rebiai *et al* applied the Finite Element Method (FEM) using COMSOL Multiphysics software to investigate the fluid simulation of dual-frequency capacitively coupled radio-frequency discharges in helium plasma. Their findings indicated a noticeable rise in plasma potential, electron density (n_e), ion density (n_i), and electron temperature (T_e) with an increase in high frequency, suggesting significant ionization for further study

[14]. Okazaki investigated a dynamic model for an RF glow discharge, incorporating the plate geometry in parallel, and considering the transport of charged particles, including relaxation processes. The authors applied this model to an Ar discharge, investigating the plasma under high pressure and low gas temperature conditions. The results confirmed the validity of the model, indicating that it is accurate and reliable to model plasma with an RF source of 13.56 MHz [15]. FEM is nowadays widely employed to solve structural, fluid, and multiphysics problems numerically [16–19].

In this work, a FEM model of an existing RF magnetron sputtering system is developed to study plasma formation. While there are already many studies discussing the behavior of d.c. systems, the behavior of and comparison to RF systems is rather scarce. Therefore, the simulation was designed to compare the plasma parameters generated with a variation of the power input to the system for both power types. Furthermore, the influence of a permanent magnet in the magnetron was included, which also is hardly found in literature. In this case, and based on the real laboratory setup, a $Nd_2Fe_{14}B$ magnet (short: neodymium magnet) was included. With this model, parameters such as electron and ion density, electron temperature, and Debye length were calculated. The aim of this work is to offer a first step to show crucial plasma parameters that later on will have an influence on the film formation, given that these parameters might influence the quantity, energy, and trajectory of the sputtered atoms mentioned earlier. The obtained results from the simulation are compared to experimental results using a Langmuir probe. Here, the focus is put on the results of an RF system that was developed in the MatER PUCP laboratory.

2. Descriptions of the computational model

2.1. Geometric model

In the following, the geometric model is shown based on the experimental setup in figure 1. In figure 2(a), the mesh and geometry used for the simulation are shown. The magnetic as well as the electric field and the plasma formation were simulated under two different conditions: first, the cathode (the target) is connected to a d.c. potential, and second, the target is connected to an RF potential with a frequency of 13.56 MHz, which is common for RF magnetron sputtering [5]. To obtain accurate results for the elastic and inelastic collisions of ions and electrons, a mesh size was defined that led to conclusive results in reasonable computing times. A minimum mesh element size of 6.0×10^{-5} m was used near the target region, while a maximum element size of 0.0134 m was set near the chamber walls. This mesh distribution allowed for accurate resolution of the plasma behavior in critical areas while maintaining computational efficiency. The generated mesh consists of 21,121 triangular elements, 14,250 quadrilateral elements, and 1,713 edge elements. To evaluate the influence of the mesh on the accuracy of the results, a mesh refinement process was carried out during model development. The mesh was progressively refined, and it was observed that further refinement did not produce noticeable changes in key plasma parameters such as electron density and electric potential. Based on these observations, we estimate that the variation introduced by mesh resolution is less than 2–3%. Therefore, the final mesh was selected to ensure both computational efficiency and numerical stability.

This led to a computing time of 7 minutes and 19 seconds for the d.c. experiment and 19 minutes and 34 seconds for the RF experiment. The plasma formation within the first 1μs of the sputtering experiment was analyzed, assuming that the process is stable for process times longer than this. The red line in figure 2(b) represents the position at which the data was analyzed to compare d.c. and RF magnetron sputtering and is close to the position of the Langmuir probe. These simulated results were obtained using an HP OMEN 15 laptop with an Intel(R) Core(TM) i7-10750H CPU @ 2.60 GHz 2.59 GHz processor and 16 GB of installed RAM with the COMSOL license number 6090309 and version 6.1.

In this work, a two-dimensional fluid model was used, due to the geometry of the sputtering system. The model is based on the parameters of the real experiment in the magnetron sputtering system. Argon was chosen as the sputtering gas, as this was also used in the experimental setup in the laboratory. The simulations were performed using COMSOL Multiphysics version 6.1, which allows time-dependent resolution of low-pressure plasmas.

The present model involves the module for plasma with the magnetic field with no current. In the first step, the magnetic field distribution is computed using the *Magnetic Fields, No Currents* module, based on the experimental geometry and the neodymium permanent magnet configuration shown in figure 4(a). This magnetic field remains constant over time and is then coupled into the plasma module.

The electric field, obtained in the presence of this static magnetic field, is used as the initial condition in the time-dependent plasma simulation. It is necessary to take these values to start modeling the plasma. It is essential to note that the plasma model depends on the magnetic field values generated by neodymium magnets. The values of the magnets are computed in a stationary state. In contrast, the plasma model was developed using time-dependent computing. Initial and boundary conditions were defined according to the experimental

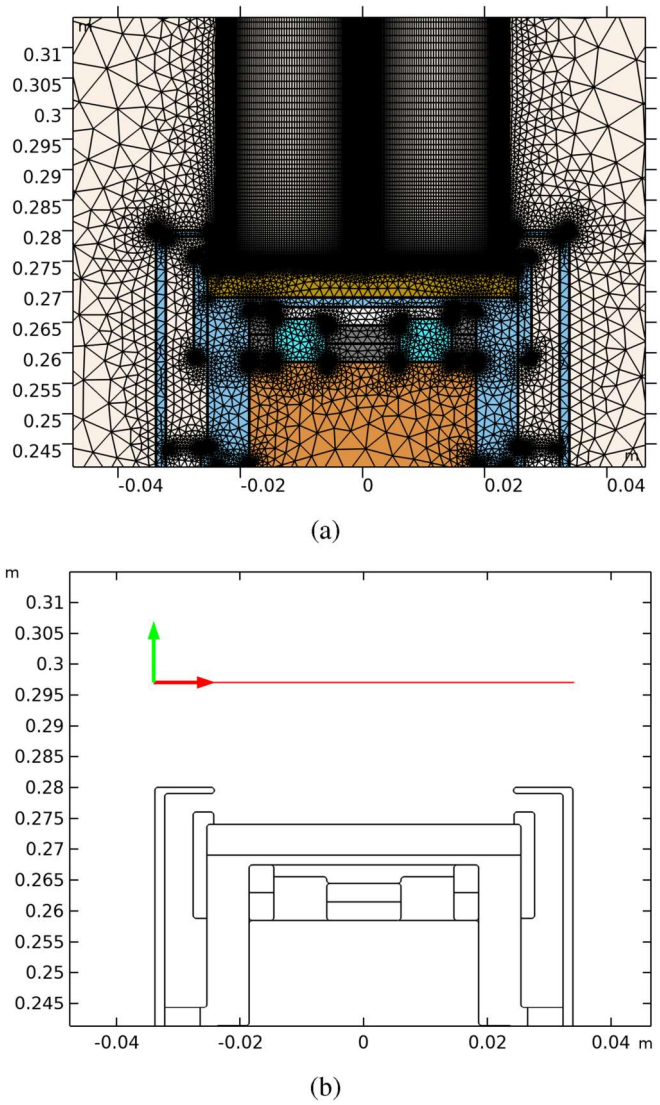

Figure 2. (a) Mesh generated with FEM for the magnetron sputtering system. (b) Data line for the analysis of the plasma parameters at 23 mm distance from the target.

configuration. In the d.c. case, a constant voltage is applied, whereas in the RF mode, a sinusoidal signal of 13.56 MHz is used, as in the laboratory setup.

The simulation was carried out for an argon discharge operating at a pressure of 1 Pa and created by a power variation between 20 W and 90 W. For both the RF and d.c. modes, a target diameter of 2 inches was used in the simulations, since the experimental target in the laboratory has this exact size. Additionally, optical emission spectroscopy measurements, which will be presented in a forthcoming paper, complement the Langmuir probe diagnostics. These parameters correspond to the laboratory's RF magnetron system operating under these experimental conditions, so the values obtained with FEM in RF mode will be compared with those obtained using the Langmuir probe.

2.2. Descriptions of the computational model

The modeling approach used in this paper is fluid to describe the particle transport by d.c. and RF power. The module uses the Poisson equation and the first two moments of the Boltzmann equation to determine each species's density, momentum, and energy (ions and electrons) [20].

In this model, the argon plasma is formed of electrons *e*, positively charged argon ions (Ar^+), argon atoms in a metastable state (Ars), and neutral argon atoms (Ar). These constituents can be described using the continuity equation:

$$\frac{\partial(n_e)}{\partial t} + \nabla \cdot \Gamma_e = k_i n_e N \tag{1}$$

$$\frac{\partial(n_p)}{\partial t} + \nabla \cdot \Gamma_p = k_i n_e N \tag{2}$$

$$\frac{\partial(n_*)}{\partial t} + \nabla \cdot \Gamma_* = k_{ex} n_e N \tag{3}$$

Where $\Gamma_e, \Gamma_p, \Gamma_*$ represent the flux of each particle, the subindex e denotes electrons, p denotes positive ions Ar^+, * denotes metastable atoms Ars, N is the density of neutral gas, K_i is the ionization rate coefficient, and K_{ex} is the excitation rate coefficient [14]. The rate coefficients for process j, where j represents either ionization (i) or excitation (ex), are defined by:

$$K_j = \int_0^\infty f(\epsilon)\sigma_j(\epsilon)\nu(\epsilon)\, d\epsilon \tag{4}$$

Here, ϵ denotes the electron energy, σ_j denotes collision cross-section, ν represents electron velocity, and $f(\epsilon)$ denotes the electron energy distribution function (EEDF). A Maxwellian distribution function can approximate the electron energy distribution function (EEDF), as described in [21]. This distribution is used in this paper to enhance computational efficiency. The simulation of electron density and mean electron energy involves solving a pair of drift-diffusion equations, as outlined in work by Uchida *et al* [22]. The average electron energy measured in volts (V) is equivalent to the average electron energy expressed in electronvolts (eV) and is obtained by dividing it by the elementary charge [20]. The equation for electron density is explicitly provided in the documentation by [23]:

$$\frac{\partial(n_e)}{\partial t} + \nabla \cdot \Gamma_e = R_e - (\mathbf{u} \cdot \nabla) n_e \tag{5}$$

$$\Gamma_e = -(\mu_e \bullet \mathbf{E}) n_e - \nabla(\mathbf{D}_e n_e) \tag{6}$$

In the context of the following expressions, n_e represents the electron density ($1/m^3$), R_e is the rate expression for electrons ($1/m^3 \cdot s$), μ_e represents electron mobility which can be a scalar or a tensor ($m^2/V{\cdot}s$), $\mathbf{D}_e$ denotes electron diffusivity (m^2/s), $\mathbf{E}$ stands for the electric field (V/m), $\mathbf{u}$ represents the neutral fluid velocity (m/s), and Γ_e is the electron flux density. The expression for electron energy density can be found in the documentation by [23].

$$\frac{\partial(n_\epsilon)}{\partial t} + \nabla \cdot \Gamma_\epsilon + \mathbf{E} \cdot \Gamma_\epsilon = S_{en} - (\mathbf{u}.\nabla) n_\epsilon + \frac{(Q + Q_{gen})}{q} \tag{7}$$

$$\Gamma_\epsilon = -(\mu_\epsilon \bullet \mathbf{E}) n_\epsilon - \nabla(\mathbf{D}_\epsilon n_\epsilon) \tag{8}$$

Where n_ϵ represents the electron energy density (V/m^3), μ_ϵ signifies the electron energy mobility ($m^2/V{\cdot}s$), S_{en} denotes the energy loss/gain due to inelastic collisions ($V/m^3{\cdot}s$), $\mathbf{D}_\epsilon$ stands for electron energy diffusivity (m^2/s), Q represents the external heat source, and Q_{gen} is the generalized warmness source (W/m^3). The mean electron energy, denoted as $\bar{\epsilon}$ is determined using the expression in V:

$$\bar{\epsilon} = \frac{n_\epsilon}{n_e} \tag{9}$$

The difference in mobility and diffusivity between ions and electrons creates a separation of space charge in the plasma sheath. Utilizing the following equation for a quantity results in the temperature of electrons (T_e) in volts [23]:

$$T_e = \frac{2}{3}\bar{\epsilon} \tag{10}$$

The plasma module will take data from the magnetic field. The magnetic field equations used Maxwell's equations, which describe the behavior of electric and magnetic fields. These equations are essential for understanding and predicting the behavior of electromagnetic waves and the behavior of materials in electromagnetic fields. Maxwell's equations must be written with a set of specified conditions [24].

$$\nabla \cdot \mathbf{D} = \rho \tag{11}$$

$$\nabla \cdot \mathbf{B} = 0 \tag{12}$$

$$\nabla \times \mathbf{E} = -\frac{\partial \mathbf{B}}{\partial t} \tag{13}$$

$$\nabla \times \mathbf{H} = \mathbf{J} + \frac{\partial \mathbf{D}}{\partial t} \tag{14}$$

In the presented context, $\mathbf{B}$ represents the electric field intensity, $\mathbf{D}$ denotes the electric displacement or electric flux density, $\mathbf{H}$ signifies magnetic field intensity, $\mathbf{B}$ stands for magnetic flux density, $\mathbf{J}$ represents current density, and ρ corresponds to electric charge density. This modeling procedure is initiated by applying the first of Maxwell's equations. Magnets, specifically those crafted from ferromagnetic material, inherently generate magnetic fields without requiring the presence of current.

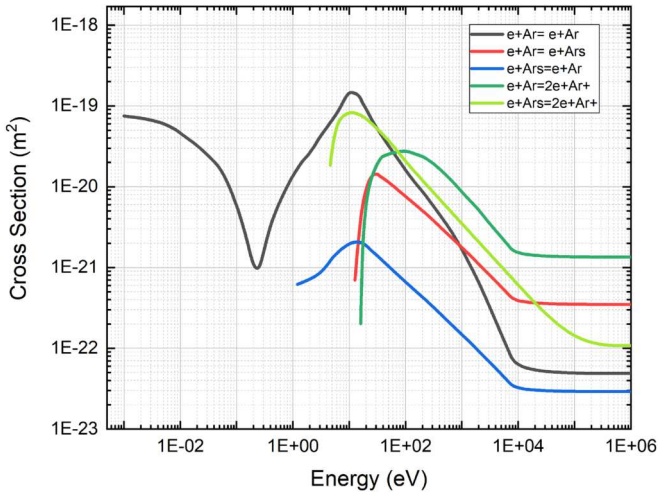

Figure 3. Cross-section data depicting electron impact reactions with argon gas [23].

Table 2. List of modeled collisions and reactions.

Reactions	Type	ε (eV)	References
$Ar + e \rightarrow Ar + e$	Elastic	0	[25]
$Ar + e \rightarrow Ars + e$	Excitation	11.5	[26]
$Ars + e \rightarrow Ar + e$	Superelastic	−11.5	[27]
$Ar + e \rightarrow Ar^{+} + 2e$	Ionization	15.8	[28]
$Ars + e \rightarrow Ar^{+} + 2e$	Ionization	4.24	[29]
$Ars + Ars \rightarrow Ar^{+} + Ar + e$	Penning ionization	—	[30]
$Ars + Ar \rightarrow Ar + Ar$	Metastable quenching	—	[27]

$$\nabla \times \mathbf{H} = 0 \tag{15}$$

$$\mathbf{H} = -\nabla V_m \tag{16}$$

Lastly, the simultaneous system of equations to be solved is as follows:

$$\nabla \cdot \mathbf{B} = 0 \tag{17}$$

$$\mathbf{B} = \mu_0 \mu_r \mathbf{H} \tag{18}$$

The input parameter for the model is denoted as the magnetic scalar potential (V_m), serving as a domain condition, specifically in scenarios where no current contributes to the magnetic field. This condition is essential in defining the magnetic field distribution across all domains. The symbols μ_0 and μ_r refer to the magnetic permeability values for a vacuum and a specific material, including the relative magnetic permeability of the material, respectively.

2.3. Plasma reactions

There are more than five reactions that are considered part of the plasma study, which includes elastic and inelastic collisions, as shown in table 2 [23]. Furthermore, figure 3 illustrates the velocity coefficients for the first five reaction processes occurring in the system under low-pressure conditions.

Argon is a favorable choice for a benchmark problem due to its simplicity, involving a limited number of reactions and species. The specific chemical reactions under consideration are detailed, with electron impact cross-sections provided in table 2.

At the beginning of the process, a limited number of initial electrons are present, playing a crucial role in forming the discharge during the initial RF cycle or when using d.c. power. In addition to volumetric reactions, the model also incorporates two surface reactions. These are conditions applied at the walls to prevent a decrease in ion density values. Since the model does not simulate a constant argon flow as it would occur experimentally, it still provides acceptable values for ion density, electron density, electron temperature, and Debye length—typical parameters of plasma diagnostics. When ions reach the wall, they are assumed to revert to neutral argon atoms, transferring their charge to the wall (the cathode is referred to as a metal contact in the

Table 3. Table of surface reactions used in the model [23].

Reaction	Formula	Sticking coefficient
1	$Ars \rightarrow Ar$	1
2	$Ar^{+} \rightarrow Ar$	1

Table 4. Table of boundary conditions used in the model [23].

Boundary conditions		
SEE	0.20	
Initial $n_{e,0}$	1.00×10^{15}	m^{-3}
Initial $\bar{\epsilon_0}$	3	V
Initial electric potential	0	V

model). The values from table 3 have been employed throughout the Plasma Module model, as applied to the cathode in the magnetron sputtering configuration.

The primary boundary conditions for the simulation are detailed in table 4. These initial conditions are important since the parameters are close to those used experimentally in the MatER laboratory, where an aluminum target with argon gas is used for RF magnetron sputtering. The value of the secondary electron emission coefficient (SEE) used in the simulations is taken for an aluminum target [31].

3. Results and discussion

3.1. Electric and magnetic field

The magnetic scalar potential is used, with a specific value of $\pm$ 250 A chosen to approximate the magnetic fields produced by $Nd_2Fe_{14}B$ magnets. These magnets typically operate within a maximum range of 0.97 T, a value experimentally used in the MatER (Materials Science and Renewable Energies Research) laboratory. In figure 4(a), the distinctive streamlines representing a cylindrical magnetron are shown, emphasizing the significance of the magnet polarity's placement in effectively confining electrons near the target, as discussed by Gudmundsson in 2020 [6].

Magnetron sputtering discharge typically operates in the glow discharge regime. Argon is commonly used in planar d.c. magnetron sputtering sources within the pressure range of 0.2 to 4 Pa, accompanied by cathode voltages ranging from 300 to 700 V, as outlined by Gudmundsson in 2020 [6]. The cylindrical magnetron sputtering method is favored for its advantages in material conservation. In this configuration, electrons confined by the $\mathbf{E} \times \mathbf{B}$ drift contribute to enhanced ionization rates, ultimately forming thin films.

In a magnetron sputtering system, establishing a connection to an anode nearby is essential; the anode is grounded in this design. As shown in figure 4(b), a 2D cross-section illustrates that the potential is 0 V at the anode and -195 V at the cathode. The decreasing potential gradient from the cathode to the anode is pronounced. It is essential to emphasize that this configuration in the magnetron sputtering system plays a crucial role in increasing the sputtering rate on the target and prolonging the plasma duration.

3.2. d.c. and RF magnetron sputtering

Many authors have documented simulation results [6, 32–39]. The reported values vary depending on the applied potential and the pressure during the thin film formation process.

In figure 5(a) and (b), the comparison of ion density generated by magnetron sputtering is shown, where the higher ion density value is 2.06×10^{16} m^{-3} at a d.c. potential. In contrast, in RF discharges, the maximum ion density reaches 1.72×10^{16} m^{-3}. This lower density is consistent with the typical behavior of RF plasmas, where the capacitive nature of the excitation results in less efficient electron heating compared to the constant electric field in d.c. plasmas [40]. The model captures this effect through the power deposition profile and the time-dependent voltage applied at the cathode, leading to lower average electron energies and reduced ionization rates. Both cases are at a pressure of 1 Pa, generated at a power of 60 W, and the time scale of the sputtering process extends up to 1μs, during which the values were measured.

Jimenez F. conducted a study on d.c. magnetron sputtering, revealing ion densities ranging from 7.00×10^{16} m^{-3} to 3.00×10^{17} m^{-3}, applying 60 W and 240 W power, respectively. This investigation was carried out under a pressure of 2.67 Pa. The results were obtained at a distance of 5.6 cm from the Al target, and the time scale for sputtering was 1μs, during which the data were measured and found to be representative of

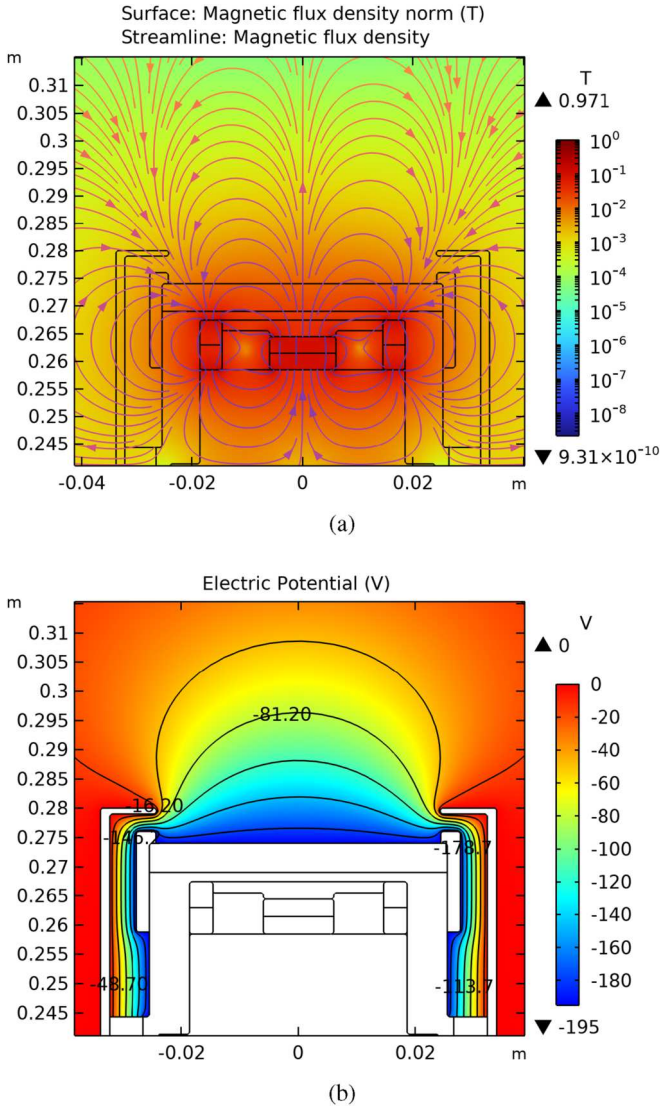

Figure 4. (a) Magnetic flux density norm in Tesla. (b) Electric potential in DC with −195 V applied at the target.

the steady-state behavior [34]. Fu Y. studied the plasma particle distribution and electron temperature in cylindrical magnetron sputtering at 1×10^{-5} s (10μs) [41].

In Radiofrequency Magnetron Sputtering (RFMS), the plasma remains stable within 1μs. Nevertheless, due to the computational demands of the plasma model, obtaining results beyond 1μs—such as up to 10μs—would require over a week of processing time. Therefore, the comparison between d.c. and RF discharges is conducted under a steady-state plasma regime, specifically at 1μs after plasma ignition near the substrate, as demonstrated in the presented results. Matyash investigated atom confinement under RF power. The results, obtained using a Langmuir probe at a pressure of 8.00 Pa, a power of 120 W, a frequency of 13.56 MHz, and a distance of 2.5 cm from the cathode, showed a plasma density of 2.55×10^{16} m^{-3}. This value was measured at a radial distance of 2 cm from the aluminum target [35].

Figure 6(a) and (b) show the comparison of the $\mathbf{E} \times \mathbf{B}$ drift velocity. This drift allows electrons to remain close to the target for a longer period, thereby increasing ionizing collisions. The results show that using d.c. or RF power can achieve higher concentrations of electron confinement near the target. The continuous d.c. potential can confine more electrons near the target. The green color of the confinement values represents negative velocity as they move backward from the page, and red indicates positive velocity as they move toward the reader. Zheng B. conducted simulations using particle-in-cell (PIC) and Monte Carlo collision techniques to analyze both 1D and 2D scenarios in a balanced Direct Current Magnetron Sputtering (DCMS) discharge, revealing particle confinement induced by the $\mathbf{E} \times \mathbf{B}$ drift. These findings were obtained under specific conditions, including a target with a thickness of 60 mm and a diameter of 55 mm, operating at a pressure of 0.6 Pa [42]. In the DCMS system with a magnetic field strength of 0.025 T (the maximum value), Zheng observed that

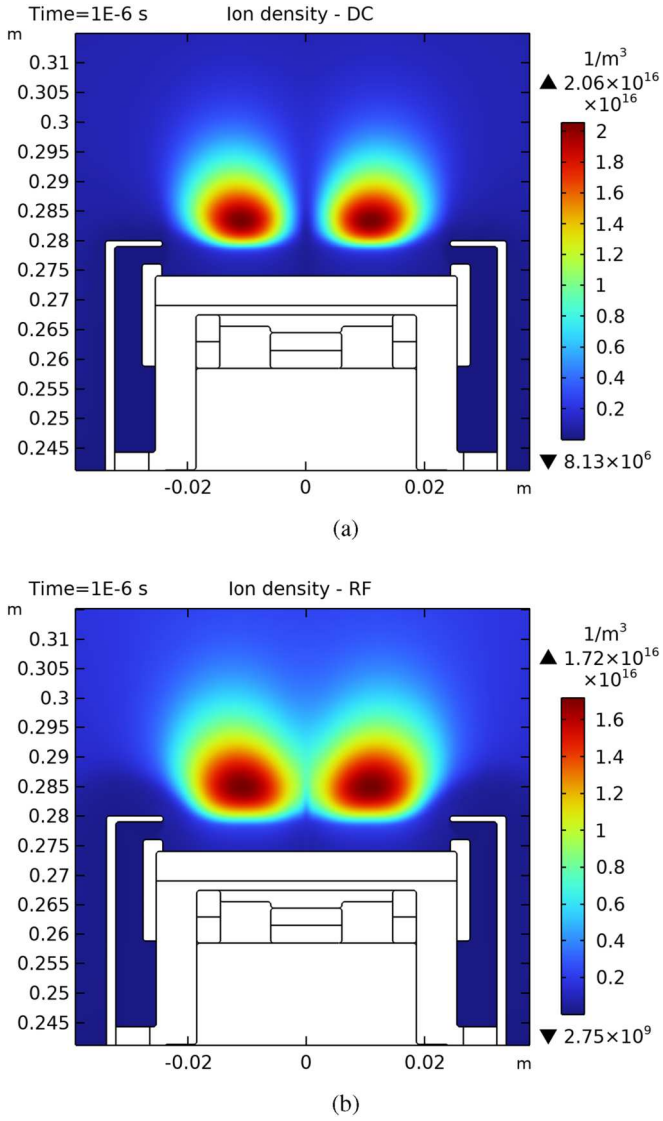

Figure 5. (a) Ion density in DCMS on a linear scale at 1 μs. (b) Ion density in RFMS on a linear scale at 1 μs.

the target erosion profile follows a Gaussian distribution, with the peak located beneath the region of maximum plasma density (1.20×10^{16} m^{-3}).

The difference in plasma density between both magnetron configurations can be attributed to essential factors such as the type of applied potential, frequency, pressure, target material, and magnetic field design, which in turn influence the ionization and plasma density in the sputtering process.

The ion density for DCMS and RFMS can be seen in figure 7(a) and (b), where it is observed that as the potential increases, the values increase progressively and are confined near the center of the target due to the magnetic and electric fields, with a decrease towards the target edges. In this peripheral zone, the electron confinement is weaker, leading to an ion density increase from 0.99×10^{15} m^{-3} to 1.41×10^{17} m^{-3} in intensity, with values measured at a radius of $x = \pm$ 0.010 m in DCMS, and from 1.95×10^{15} m^{-3} to 1.95×10^{16} m^{-3} in RFMS.

The values obtained for both ion and electron densities are within the same order of magnitude, supporting the assumption of a quasineutral plasma in both RF and d.c. modes. The presence of two peaks in ion and electron densities during the magnetron sputtering process is associated with the magnet configuration [41]. These magnets confine the charged particles and enhance plasma discharge efficiency. As a result, an asymmetric plasma distribution is formed, with two distinct density peaks. These values increase as the voltage applied to the cathode rises and vary as a function of the distance between the cathode and the substrate. The magnetron sputtering system produces non-uniform ion and electron densities due to the interaction between the electric and magnetic fields.

The increase in the ionization rate values in both processes when the power increases may be associated with the interaction of energy with electrons. As shown in figure 8(a), there is an increase in the range from

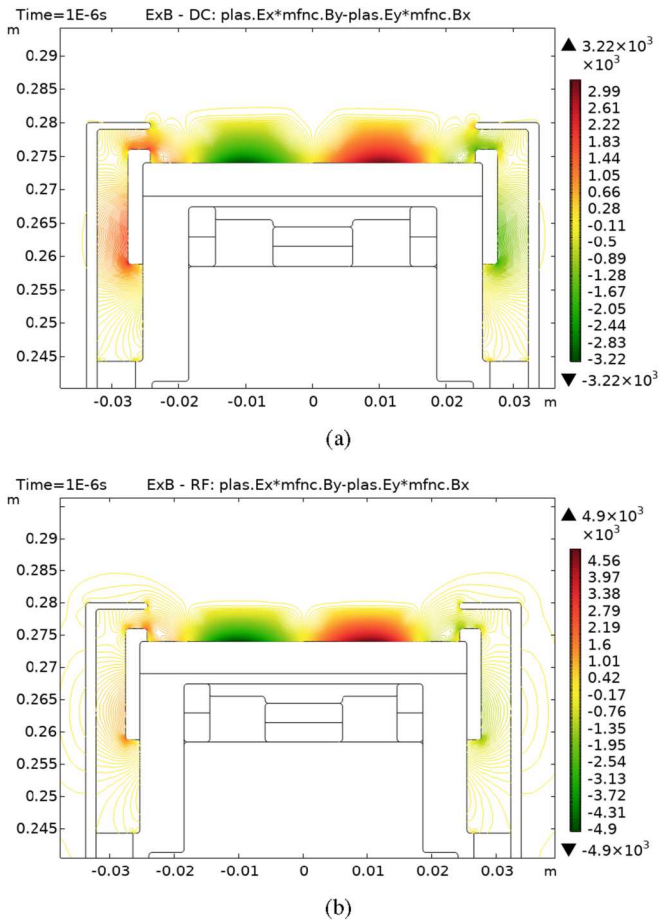

Figure 6. (a) **E** × **B** drift generated in DCMS. (b) **E** × **B** drift obtained in RFMS with a linear scale.

5.97×10^{-3} mol/(m$^3 \cdot$ s) to 7.80×10^{-2} mol/(m$^3 \cdot$ s) for DCMS and from 1.30×10^{-4} mol/(m$^3 \cdot$ s) to 1.61×10^{-1} mol/(m$^3 \cdot$ s) for RFMS.

These values are higher in the region of electron confinement than in the center. These values are also obtained for the magnetic field configuration. Increasing the power in magnetron sputtering provides more energy to the system. This additional energy can result in greater ionization of the atoms in the plasma, generating a greater number of free electrons. An increase in ionization values is also observed with increasing power. This increase can enhance the mobility of electrons in the plasma, allowing them to contribute more effectively to the electron ratio and, consequently, to ionization.

Tables 5 and 6 present an analysis of values obtained from d.c. and RF modes, focusing on parameters such as plasma density, electron temperature, Debye length, and metastable argon population. The data reveal several significant differences between the two methods.

Regarding plasma density, DCMS consistently yields higher values compared to RFMS. This trend suggests that the continuous energy supply in d.c. mode facilitates a steadier sputtering process, resulting in higher deposition rates and denser films on the substrate.

Electron temperature, a key parameter influencing plasma behavior, decreases with increasing power in both d.c. and RF modes. This reduction can be attributed to the enhanced energy transfer efficiency at higher power levels, which allows the plasma to sustain itself with lower average electron energy, thus improving thermal management.

The Debye length, which characterizes the spatial scale of electric potential screening in plasmas, shows a marked decrease as power increases. This is due to the elevated plasma density at higher power, which strengthens collective particle interactions and reduces the screening distance. Furthermore, the population of metastable argon atoms grows with increasing discharge power. This increase is linked to higher electron densities and energies, which promote excitation of ground-state argon atoms to long-lived metastable states. Given the low de-excitation rates of these states—due to radiative transition constraints—their accumulation becomes more significant at elevated power levels.

The ionization rate, representing the efficiency of converting neutral atoms into ions, exhibits notable differences between DCMS and RFMS. RFMS achieves higher ionization efficiency, as the alternating RF power

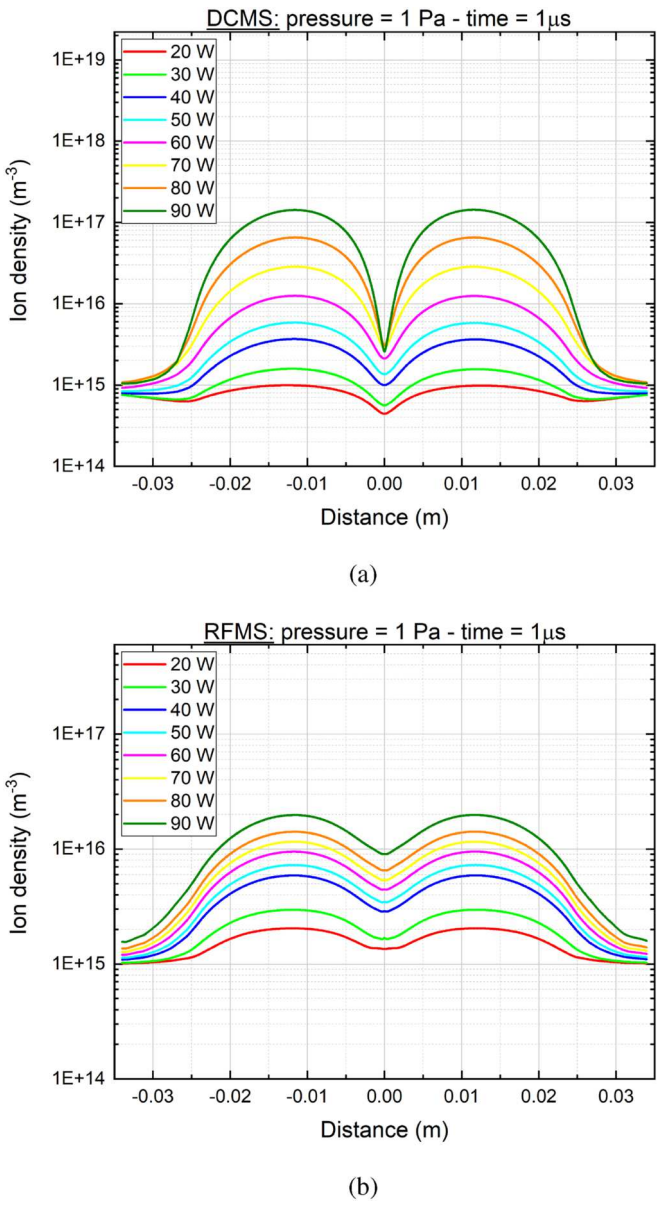

Figure 7. Ion density with power variation, data analysis in the geometry located at 23 mm distance from the target with ends on the x-axis $x = \pm 0.034$ m. (a) DCMS and (b) RFMS.

sustains the plasma more effectively by frequently accelerating electrons to energies sufficient for ionizing collisions. The rapid oscillations of the electric field in RF mode enhance ionization probability relative to the continuous d.c. case.

These findings underscore the influence of power magnitude and excitation frequency on the sputtering process. Higher power and the use of RF energy improve ionization efficiency and plasma density, which are critical for tailoring coating properties. A comprehensive understanding of these differences enables better control and optimization of sputtering parameters, ultimately enhancing material quality and performance across diverse applications.

Figure 9 presents the data obtained using a simple Langmuir probe, where the electron density collected by the probe is plotted as a function of the increasing RF power applied to the aluminum target. These experimental results are compared with numerical values obtained from finite element method (FEM) simulations performed in RF mode.

A systematic increase in the electron saturation current is observed as the applied power increases. This behavior indicates a corresponding rise in plasma electron density. The higher energy input enhances the ionization rate of the background gas, leading to a greater concentration of free electrons in the discharge chamber.

The observed increase in electron saturation current with increasing RF power confirms the expected correlation between energy input and plasma density. As the power applied to the aluminum target increases, the

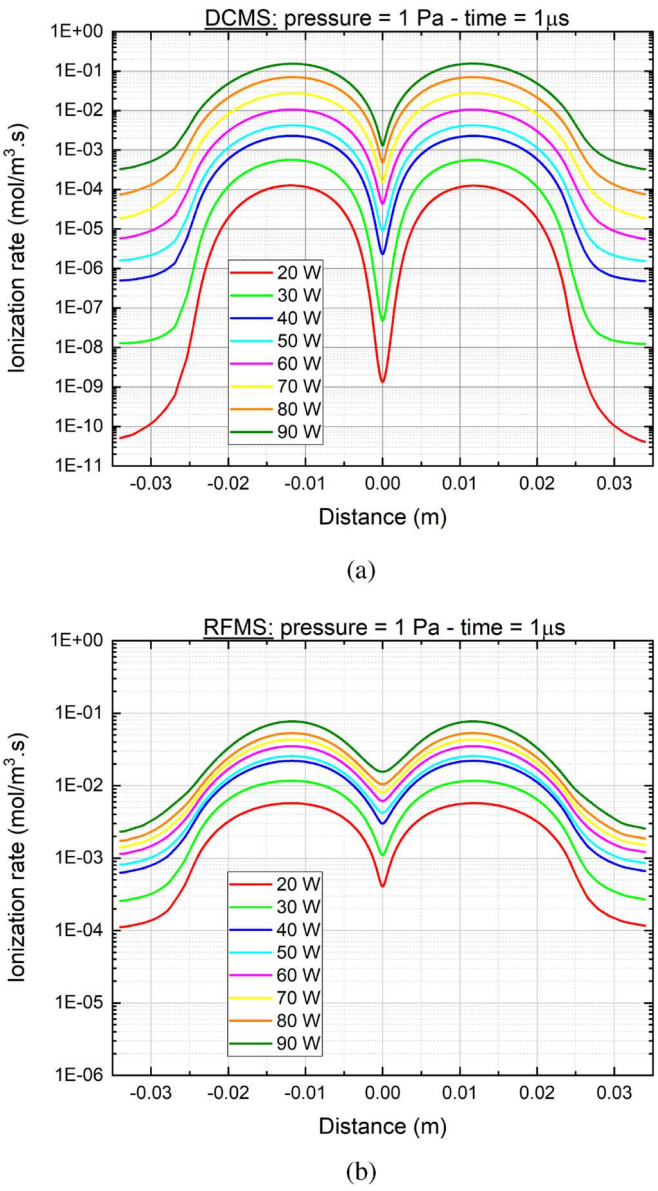

Figure 8. (a) DCMS and (b) RFMS ionization rate with power variation. Data analysis in the plasma model located at 23 mm distance from the target with ends on the x-axis at $x = \pm 0.034$ m.

Table 5. Table of DCMS power variation results at 1 μs in one point for each values taken in $y = 0.297$ m and $x = 0.010$ m.

W	$n(10^{15}\ \mathrm{m}^{-3})$	T_e(eV)	$\lambda_D(10^{-4}\ \mathrm{m})$	Ars $(10^{15}\ \mathrm{m}^{-3})$
20	0.99	5.28	4.29	0.17
30	1.61	5.24	3.79	0.95
40	3.64	5.12	2.63	2.60
50	5.83	4.93	2.13	3.96
60	12.70	4.73	1.50	7.26
70	28.17	4.57	1.01	13.22
80	66.13	4.00	0.68	23.75
90	141.34	3.27	0.45	42.36

ionization efficiency improves, resulting in a denser plasma. This is evident from the higher electron current collected in the positive voltage region of the Langmuir probe characteristic curve.

Moreover, the comparison between experimental data and FEM simulation results demonstrates strong agreement, supporting the validity of both the diagnostic method and the computational model used. These

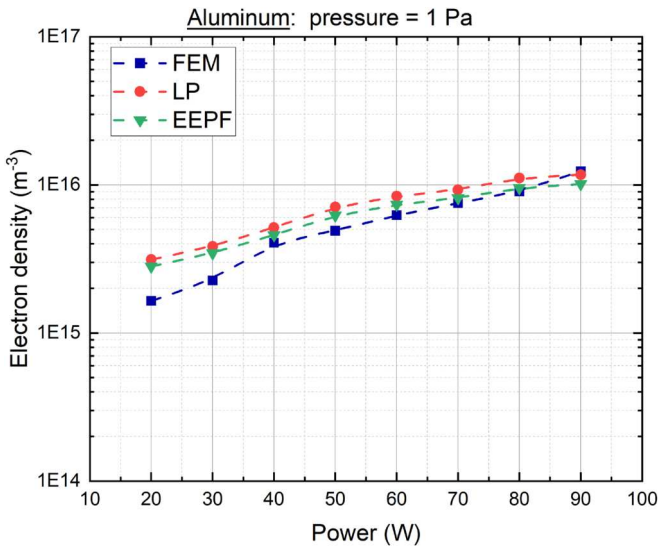

Figure 9. Experimental data obtained with the Langmuir probe in RF magnetron sputtering at a distance from the aluminum target of 23 mm.

Table 6. Table of RFMS power variation results at 1 μs in one point for each values taken in $y = 0.297$ m and $x = 0.010$ m.

W	$n(10^{15}\ \mathrm{m}^{-3})$	T_e(eV)	$\lambda_D(10^{-4}\ \mathrm{m})$	Ars $(10^{15}\ \mathrm{m}^{-3})$
20	1.95	8.12	4.42	0.63
30	2.96	8.06	3.87	1.01
40	5.81	7.96	2.75	2.47
50	7.10	7.95	2.46	2.75
60	9.28	7.94	2.15	3.60
70	11.29	7.93	1.96	4.37
80	13.92	7.90	1.76	5.34
90	19.48	6.97	1.51	7.41

findings highlight the effectiveness of combining Langmuir probe diagnostics with numerical simulations to study the behavior of RF plasmas under varying power conditions [3, 43].

4. Conclusions

In conclusion, the most significant outcomes of this work are the development of two digital twins for direct current (d.c.) and radio frequency (RF) magnetron sputtering, and their validation against experimental plasma diagnostics. These results demonstrate that the fluid modeling approach remains applicable down to pressures as low as 1 Pa. A 2D-FEM model was developed to determine the spatial distribution of plasma parameters. The study has successfully acquired detailed values of the magnetic field generated by Neodymium magnets. The importance of the magnets' configuration, size, and position in the magnetron should be emphasized, as they increase electron density and, consequently, ion density.

It has been observed that when applying direct current to magnetron sputtering, both ion density and electron density are higher compared to radio frequency power of 13.56 MHz at 1μs. These values increase as cathode power is raised, leading to an enhanced ionization rate for both d.c. and RF modes. These preliminary findings suggest that the d.c. sputtering mode may generate more favorable conditions in terms of charge densities, potentially influencing deposition properties.

The results obtained through Langmuir probe diagnostics and FEM simulations demonstrate a clear relationship between the RF power applied to the aluminum target and the resulting plasma density. As the power increases, the electron saturation current also rises, indicating a significant enhancement in electron density. This behavior is attributed to a higher ionization rate due to the increased energy input into the system. The agreement between experimental and simulated data confirms the reliability of using a simple Langmuir probe

for plasma characterization in RF discharges. These findings validate the effectiveness of combining experimental diagnostics with numerical modeling to analyze and optimize plasma generation processes.

Acknowledgments

This work was financially supported by the National Fund for Scientific and Technological Development of Peru (FONDECYT) under contract 236 − 2015, 149 − 2020, FAI −2024 and the German Academic Exchange Service (DAAD) for funding a research internship at the Institute for Applied Materials (IAM-AWP) at Karlsruhe Institute of Technology in Germany. This internship provides the software and resources necessary to complete this work.

Data availability statement

The data cannot be made publicly available upon publication because no suitable repository exists for hosting data in this field of study. The data that support the findings of this study are available upon reasonable request from the authors.

Declaration on competing interest

The authors declared that they have no known competing financial interests or personal relationships that could have appeared to influence the work reported in this paper.

Author contributions

Carlo Becerra
Software (supporting)

Jose Campo
Writing – review & editing (supporting)

Jean Carrreño 0009-0007-9828-8733
Writing – review & editing (supporting)

Humberto Torreblanca 0000-0002-1322-1545
Software (equal), Writing – review & editing (supporting)

Michael Stüber 0000-0002-6862-2418
Supervision (supporting), Writing – review & editing (supporting)

Sven Ulrich
Writing – review & editing (supporting)

Rolf Grieseler 0000-0001-5307-7755
Supervision (lead), Writing – review & editing (equal)

References

[1] Nandkumar N 2007 Plasma: The fourth state of matter *British Plastics and Rubber* **3** 6
[2] Lieberman M A, Lichtenberg A J and Wolf E L 2005 *Principles of plasma discharges concepts in nanoscienceMRS Bull.* **30** 899–901
[3] Lieberman M A and Lichtenberg A J 2005 *Principles of Plasma Discharges and Materials Processing* 1999 (MRS Bulletin) p. 4
[4] S B, Singha M K and Dwivedi P 2023 Impact of annealing on structural and optical properties of zno thin films *Microelectron. J.* **135** 105759
[5] Swann S 1988 Magnetron sputtering *Phys. Technol.* **19** 67–75
[6] Gudmundsson J T 2020 Physics and technology of magnetron sputtering discharges *Plasma Sources Sci. Technol.* **29** 113001
[7] Hala M 2011 Characterization of high power impulse magnetron sputtering *PhD Thesis* Universite De Montreal https://publications.polymtl.ca/742/219
[8] Passchier J D P and Goedheer W J 1993 Relaxation phenomena after laser-induced photodetachment in electronegative rf discharges *J. Appl. Phys.* **73** 1073–9
[9] Morton P L 1946 Ionization currents in non-uniform electric fields *Phys. Rev.* **70** 358–66

[10] Herrebout D, Bogaerts A, Yan M, Gijbels R, Goedheer W and Vanhulsel A 2002 Modeling of a capacitively coupled radio-frequency methane plasma: Comparison between a one-dimensional and a two-dimensional fluid model *J. Appl. Phys.* **92** 2290–5
[11] Herrebout D, Bogaerts A, Gijbels R, Goedheer W and Vanhulsel A 2003 A one-dimensional fluid model for an acetylene rf discharge: a study of the plasma chemistry *IEEE Trans. Plasma Sci.* **31** 659–64
[12] Herrebout D, Bogaerts A, Yan M, Gijbels R, Goedheer W and Dekempeneer E 2001 One-dimensional fluid model for an rf methane plasma of interest in deposition of diamond-like carbon layers *J. Appl. Phys.* **90** 570–9
[13] Ayub A, Hasan M and Khan M S 2022 In-situ plasma characterization of dc/rf magnetron sputtering using langmuir probe and spectroscopy *IEEE Sens. J.*
[14] Rebiai S, Bahouh H and Sahli S 2013 2-d simulation of dual frequency capacitively coupled helium plasma, using comsol multiphysics *IEEE Trans. Dielectr. Electr. Insul.* **20** 1616–24
[15] Okazaki K, Makabe T and Yamaguchi Y 1989 Modeling of a rf glow discharge plasma *Appl. Phys. Lett.* **54** 1742–4
[16] Conrads H and Schmidt M 2000 Plasma generation and plasma sources *Plasma Sources Sci. Technol.* **9** 441–54
[17] Ekpe S D and Dew S K 2006 3d numerical simulation of gas heating effects in a magnetron sputter deposition system *J. Phys. D: Appl. Phys.* **39** 1413–21
[18] Taylor R L 2000 *The Finite Element Method* (*Fluid Dynamics*) vol 3 5th edn (Butterworth-Heineman)
[19] bathe K J 1996 *Finite element procedures* **07458** 1037 pp ISBN: 0-13-301458-4
[20] Hagelaar G J and Pitchford L C 2005 Solving the boltzmann equation to obtain electron transport coefficients and rate coefficients for fluid models *Plasma Sources Sci. Technol.* **14** 722–33
[21] Franz G 2009 *Low Pressure Plasmas and Microstructuring Technology* (Springer Berlin Heidelberg) (https://doi.org/10.1007/978-3-540-78661-5)
[22] Uchida Y 1984 Dc glow discharge *Semiconductors and Semimetals* **21** 41–54 Academic Press
[23] 2018 *Comsol Multiphysics* https://www.comsol.com/plasma-module
[24] Chen F F 1984 *Introduction to Plasma Physics and Controlled Fusion* Vol. 1 (Plasma Physics) (New York, NY, USA: Springer US: Springer US) 421 pp. ISBN 978-0-306-41332-0
[25] Eggarter E 1975 Comprehensive optical and collision data for radiation action. ii. ar *J. Chem. Phys.* **62** 833–47
[26] Tachibana K 1986 *Excitation of the ls5, ls4, 1s3, and 1sz levels of argon by low-energy electrons* Physical Review A **34** 1007–15 American Physical Society (APS)
[27] Ferreira C M, Loureiro J and Ricard A 1985 Populations in the metastable and the resonance levels of argon and stepwise ionization effects in a low-pressure argon positive column *J. Appl. Phys.* **57** 82–90
[28] Straub H C, Renault P, Lindsay B G, Smith K A and Stebbings R F 1995 Absolute partial and total cross sections for electron-impact ionization of argon from threshold to 1000 ev *Phys. Rev. A* **52** 1115–24
[29] Ton-That D and Flannery M R 1977 Cross sections for ionization of metastable rare-gas atoms (ne^*, ar^*, kr^*, xe^*) and of metastable $n\,2^*$, co^* molecules by electron impact *Phys. Rev. A* **15** 517–26
[30] Kimura T and Kasugai H 2010 Experiments and global model of inductively coupled rf ar/n2 discharges *J. Appl. Phys.* **108** 8
[31] Anders A, Andersson J and Ehiasarian A 2007 High power impulse magnetron sputtering: Current-voltage-time characteristics indicate the onset of sustained self-sputtering *J. Appl. Phys.* **102** 12
[32] Wu S Z 2005 Dependence of plasma characteristics on dc magnetron sputter parameters *J. Appl. Phys.* **98** 10
[33] Held J, George M and von Keudell A 2022 Spoke-resolved electron density, temperature and potential in direct current magnetron sputtering and hipims discharges *Plasma Sources Sci. Technol.* **31**
[34] Jimenez F J 2012 *Comprehensive Simulation of Sputter Deposition* 1–301
[35] Matyash K, Fröhlich M, Kersten H, Thieme G, Schneider R, Hannemann M and Hippler R 2004 Rotating dust ring in an rf discharge coupled with a dc-magnetron sputter source. experiment and simulation *J. Phys. D: Appl. Phys.* **37** 2703–8
[36] Shidoji E, Nakano N and Makabe T 1999 Numerical simulation of the discharge in d.c. magnetron sputtering *Thin Solid Films* **351** 37–41
[37] Ekpe S D, Jimenez F and Dew S K 2006 Hybrid modeling of a DC magnetron plasma discharge *Computer Engineering* **2006**
[38] Jo Y H, Park H S, Hur M Y and Lee H J 2020 Curved-boundary particle-in-cell simulation for the investigation of the target erosion effect of dc magnetron sputtering system *AIP Adv.* **10**
[39] Vahedi V, Birdsall C K, DiPeso M A G and Ronhlien T D 1993 Capacitive rf discharges modelled by particle-in-cell monte carlo simulation. ii. comparisons with laboratory measurements of electron energy distribution functions *Plasma Sources Sci. Technol.* **2** 273–8
[40] Semenov V A, Grenadyorov A S, Oskirko V O, Zakharov A N, Rabotkin S V, Ionov I V and Solovyev A A 2019 Comparison of plasma parameters and optical emission in dc, hipims and hybrid dc+hipims modes of magnetron sputtering *J. Phys. Conf. Ser.* 1393 (Institute of Physics Publishing) 11
[41] Fu Y, Ji P, He M, Huang P, Huang G and Huang W 2023 Study of plasma particle distribution and electron temperature in cylindrical magnetron sputtering *Plasma Chem. Plasma Process.* **11** 152
[42] Zheng B, Fu Y, Wang K, Tran T, Schuelke T and Fan Q H 2021 Comparison of 1d and 2d particle-in-cell simulations for dc magnetron sputtering discharges *Phys. Plasmas* **28**
[43] Chen F F, Evans J D and Zawalski W 2012 Calibration of langmuir probes against microwaves and plasma oscillation probes *Plasma Sources Sci. Technol.* **21** 055002